HAL
open science

Origin of the large ferroelectric polarization enhancement under high pressure for multiferroic DyMnO3 studied by polarized and unpolarized neutron diffraction

Noriki Terada, Navid Qureshi, Anne Stunault, Mechthild Enderle, Bachir Ouladdiaf, Claire V Colin, Dmitry D Khalyavin, Pascal Manuel, Fabio Orlandi, Shin Miyahara, et al.

To cite this version:

Noriki Terada, Navid Qureshi, Anne Stunault, Mechthild Enderle, Bachir Ouladdiaf, et al.. Origin of the large ferroelectric polarization enhancement under high pressure for multiferroic DyMnO3 studied by polarized and unpolarized neutron diffraction. Physical Review B, 2020, 102 (8), pp.085131. 10.1103/physrevb.102.085131 . hal-04143332

HAL Id: hal-04143332

https://hal.science/hal-04143332v1

Submitted on 27 Jun 2023

HAL is a multi-disciplinary open access archive for the deposit and dissemination of scientific research documents, whether they are published or not. The documents may come from teaching and research institutions in France or abroad, or from public or private research centers.

L'archive ouverte pluridisciplinaire **HAL**, est destinée au dépôt et à la diffusion de documents scientifiques de niveau recherche, publiés ou non, émanant des établissements d'enseignement et de recherche français ou étrangers, des laboratoires publics ou privés.

Editors' Suggestion

Origin of the large ferroelectric polarization enhancement under high pressure for multiferroic $DyMnO_3$ studied by polarized and unpolarized neutron diffraction

Noriki Terada,[1,2,3,*] Navid Qureshi,[2] Anne Stunault,[2] Mechthild Enderle,[2] Bachir Ouladdiaf,[2] Claire V. Colin,[4] Dmitry D. Khalyavin,[5] Pascal Manuel,[5] Fabio Orlandi,[5] Shin Miyahara,[6] Dharmalingam Prabhakaran,[7] and Toyotaka Osakabe[8]

[1]*National Institute for Materials Science, Sengen 1-2-1, Tsukuba, Ibaraki 305-0047, Japan*
[2]*Institut Laue-Langevin, BP 156, F-38042 Grenoble Cedex 9, France*
[3]*Centre Nationale de la Recherche Scientifique, Institut Néel, 25 Avenue des Martyrs, BP 166, F-38042 Grenoble Cedex 9, France*
[4]*Université Grenoble-Alpes, Institut Néel, 25 Avenue des Martyrs, BP 166, F-38042 Grenoble Cedex 9, France*
[5]*ISIS Facility, STFC Rutherford Appleton Laboratory, Chilton, Didcot, Oxfordshire OX11 0QX, United Kingdom*
[6]*Department of Applied Physics, Fukuoka University, 8-19-1 Nanakuma, Jonan-ku, Fukuoka 814-0180, Japan*
[7]*Clarendon Laboratory, Department of Physics, University of Oxford, Parks Road, Oxford OX1 3PU, United Kingdom*
[8]*Japan Atomic Energy Agency, Tokai, Ibaraki 319-1195, Japan*

(Received 3 April 2020; accepted 29 July 2020; published 14 August 2020)

The multiferroic perovskite rare earth manganites $R\mathrm{MnO_3}$ ($R =$ Dy, Tb, Gd) are known as multiferroics exhibiting pressure-induced gigantic ferroelectric polarization. In this study, we have investigated the magnetic orderings in the pressure-induced phases for $DyMnO_3$, by neutron diffraction and spherical neutron polarimetry (SNP) experiments up to 8.0 GPa. The magnetic ordering for Mn spins changes from the incommensurate *bc*-cycloid to the commensurate collinear *E*-type structure with $\boldsymbol{k}_{\mathrm{Mn}} = (0, \frac{1}{2}, 0)$ above 4.0 GPa, which is concomitant with the appearance of a giant ferroelectric polarization. The magnetic ordering for the Dy spins has been determined to be a noncollinear spin structure with *a* and *b* spin components and $\boldsymbol{k}_{\mathrm{Dy}} = (0, \frac{1}{2}, 0)$ for the low- and high-pressure phases. The magnetic field along the *a* axis, H_a, affects the Dy ordering, which is seen in the changes in the $\boldsymbol{k}$ vector from $\boldsymbol{k}_{\mathrm{Dy}} = (0, \frac{1}{2}, 0)$ in $H_a \leqslant 3$ T to $\boldsymbol{k}_{\mathrm{Dy}} = (0, 0, 0)$ in $H_a \geqslant 3$ T. Considering the lattice distortion generated by the determined magnetic orderings through the exchange striction mechanism, we conclude that the exchange striction for rare earth and Mn bonds, which is added to the uniform polarization generated by the *E*-type Mn ordering, is strongly related to the significant magnetic field enhancement of ferroelectric polarization in the high-pressure phase of the rare earth manganites.

DOI: 10.1103/PhysRevB.102.085131

I. INTRODUCTION

Type-II multiferroics, which possess ferroelectric polarization driven by magnetic order, have been intensively studied in the last 15 years [1,2]. Since the multiferroics mostly exhibit small ferroelectric polarization (<0.1 μC/cm^2), the polarization value is hoped to be the same order as that of conventional ferroelectric materials, such as $BaTiO_3$, from the practical application point of view. Recently, the largest ferroelectric polarization, ~1.0 μC/cm^2, in type-II multiferroics has been reported in the high-pressure phases of orthorhombic perovskites $R\mathrm{MnO_3}$ ($R =$ Tb, Dy, Gd), which is nearly comparable to conventional ferroelectric materials [3,4]. The ferroelectric polarization is also largely enhanced by the application of a magnetic field in the manganites. Previous neutron diffraction experiments under high pressure for $TbMnO_3$ proved that the collinear *E*-type magnetic ordering for Mn spins with the commensurate propagation vector, $\boldsymbol{k}_{\mathrm{Mn}} = (0, \frac{1}{2}, 0)$ (*Pbnm* setting), is induced in the high-pressure phase [5,6]. The first-principles calculations inferred that the exchange striction for the *E*-type ordering can be the origin of the giant ferroelectricity in $R\mathrm{MnO_3}$ [3]. However, the magnetic field enhancement of the ferroelectric polarization in the high-pressure phases of $R\mathrm{MnO_3}$ has not been understood so far.

For $DyMnO_3$, incommensurate noncollinear *bc*-cycloid ordering of Mn spins with $\boldsymbol{k}_{\mathrm{Mn}} = (0, 0.37, 0)$ appears below $T_{\mathrm{N2}}^{\mathrm{Mn}} = 18$ K and breaks the inversion symmetry, leading to spontaneous electric polarization along the *c* axis, at ambient pressure [7,8], as illustrated in the schematic phase diagram in Fig. 1. Collinear spin-density-wave (SDW) ordering exists for $T_{\mathrm{N2}}^{\mathrm{Mn}} \leqslant T \leqslant T_{\mathrm{N1}}^{\mathrm{Mn}} = 38$ K [9–11]. In the cycloid phase, the incommensurate spin modulation of Dy spins is also induced at the same $\boldsymbol{k}$ vector as the Mn ordering [7,8]. Below $T_{\mathrm{N}}^{\mathrm{Dy}} = 6.5$ K, the $\boldsymbol{k}$ vector for Dy ordering in $DyMnO_3$ is commensurate, $\boldsymbol{k}_{\mathrm{Dy}} = (0, \frac{1}{2}, 0)$, even at ambient pressure, which is different from the incommensurate $\boldsymbol{k}$ vector for Tb ordering in $TbMnO_3$ [12–14]. We thus anticipate that the comparison in pressure and magnetic field effect on magnetic ordering between $TbMnO_3$ and $DyMnO_3$ is important for understanding the enhancement of ferroelectric polarization in $R\mathrm{MnO_3}$. In this study, we have investigated the pressure and magnetic field dependence of magnetic orderings in $DyMnO_3$ by means

*TERADA.Noriki@nims.go.jp

 ©2020 American Physical Society

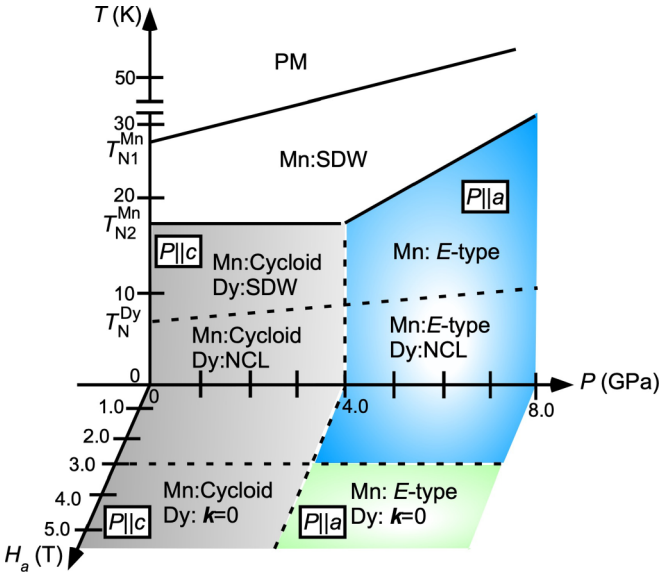

FIG. 1. Schematic illustration of the magnetic phase diagram as functions of temperature, pressure, and magnetic field along the a axis in $DyMnO_3$. "NCL" is an abbreviation for "noncollinear" state.

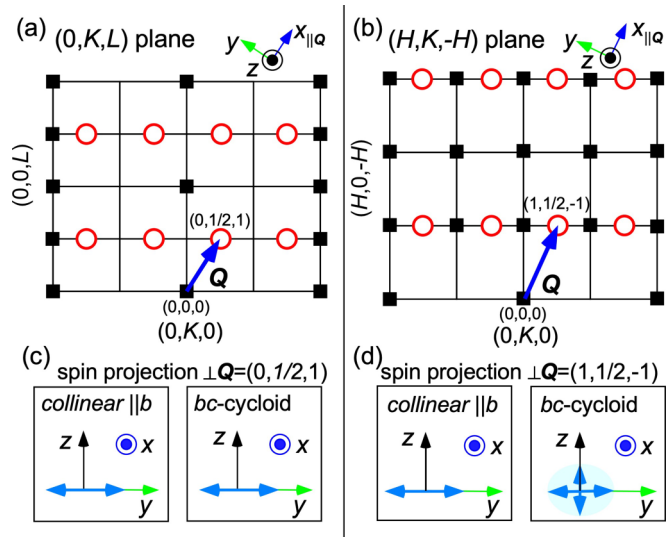

FIG. 2. Schematic drawings of the reciprocal lattice (a) $(0, K, L)$ and (b) $(H, K, \bar{H})$ planes in the spherical neutron polarimetry experiments. x, y, z axes denote directions of the neutron polarization axis. Square and circle dots denote positions of nuclear reflections allowed in the $Pbnm$ space group, and magnetic reflections expected from the E-type magnetic structure for Mn spins in the high-pressure phase in $DyMnO_3$. Relationships between spin projections perpendicular to $\boldsymbol{Q}$ and neutron polarization directions for the experimental setups with (c) $(0, K, L)$ and (d) $(H, K, \bar{H})$ scattering planes. While the spin projections of the collinear structure with spins along the b axis and bc-cycloid structure are the same for $\boldsymbol{Q} = (0, \frac{1}{2}, 1)$ on the $(0, K, L)$ plane, they are distinguishable for $\boldsymbol{Q} = (1, \frac{1}{2}, -1)$ on the $(H, K, \bar{H})$ plane.

of a neutron diffraction and spherical neutron polarimetry (SNP) analysis under high pressure.

The SNP experiment is known as a powerful technique for determining precise magnetic structure parameters in complex magnetic structures even for compounds including elements with large neutron absorption, such as Gd and Dy [15–17]. However, a combination of this technique and a high-pressure condition has been difficult, because the sample space is completely nonmagnetic to avoid neutron depolarization. Recently, we have developed a nonmagnetic hybrid anvil cell (HAC) specialized for SNP experiments, which has made the combination of SNP and high-pressure condition possible [18,19]. Here, we show the results of the SNP analysis as well as unpolarized neutron diffraction experiments under high pressure up to 8.0 GPa for multiferroic $DyMnO_3$.

II. EXPERIMENTAL DETAILS

Single-crystal samples of $DyMnO_3$, grown by the floating-zone method, were cut into a platelike shape with dimensions $0.6 \times 0.5 \times 0.18$ mm^3 (0.054 mm^3) (sample 1) for high-pressure measurements and ~5 mm^3 (sample 2) for ambient pressure experiments. The SNP experiments were performed using the CRYOgenic Polarization Analysis Device apparatus [15,16] on the IN20 beamline at the Institute Laue Langevin (ILL) in Grenoble, France. The incident neutron wavelength 1.53 Å was employed. We used the recently developed nonmagnetic HAC made of CuBe alloys with sapphire and WC (Ni-binder) anvils, which are described in detail elsewhere [18,19]. We chose two scattering planes, $(0, K, L)$ and $(H, K, \bar{H})$, for the SNP experiments, in order to see the difference in spin projection perpendicular to the scattering vector $\boldsymbol{Q}$ between the collinear and spiral structures. Relationships between the crystal lattice orientation and neutron spin polarization axes in the $(0, K, L)$ and $(H, K, \bar{H})$ planes for the SNP experiment are drawn in Figs. 2(a) and 2(b). Since the SNP analysis is only sensitive to spin projections perpendicular to $\boldsymbol{Q}$ [20], some similar magnetic structures are not distinguishable for one scattering plane experiment. For example, as illustrated in Figs. 2(c) and 2(d), the collinear structure with spins along the b axis and bc-cycloid structure are not distinguishable in the $(0, K, L)$ plane, while they give different spin projections in the $(H, K, \bar{H})$ plane. The polarization matrices in the SNP analysis were calculated with the MAG2POL program [20]. For unpolarized neutron diffraction experiments under high pressure and high magnetic field, we used the time-of-flight diffractometer WISH at the ISIS Facility, U.K. [21]. The vertical field cryomagnet was used to apply the magnetic field along the a axis in the experiment on WISH. The neutron Laue diffractometer Cyclops at ILL was also used. We also used the HAC for these unpolarized neutron experiments. We employed liquid glycerin for the pressure transmission medium. During the loading pressure for 8.0 GPa, the cell was heated to ~100 °C to keep the glycerin in a liquid state [22]. Pressure values were determined by the ruby fluorescence method at room temperature.

III. EXPERIMENTAL RESULTS

A. Pressure and magnetic field dependence of magnetic orderings

Magnetic reflections, indexed as $\boldsymbol{Q} = (0, k, -1)$ and $(1, 1-k, -1)$ with the incommensurate $k = 0.37$, are

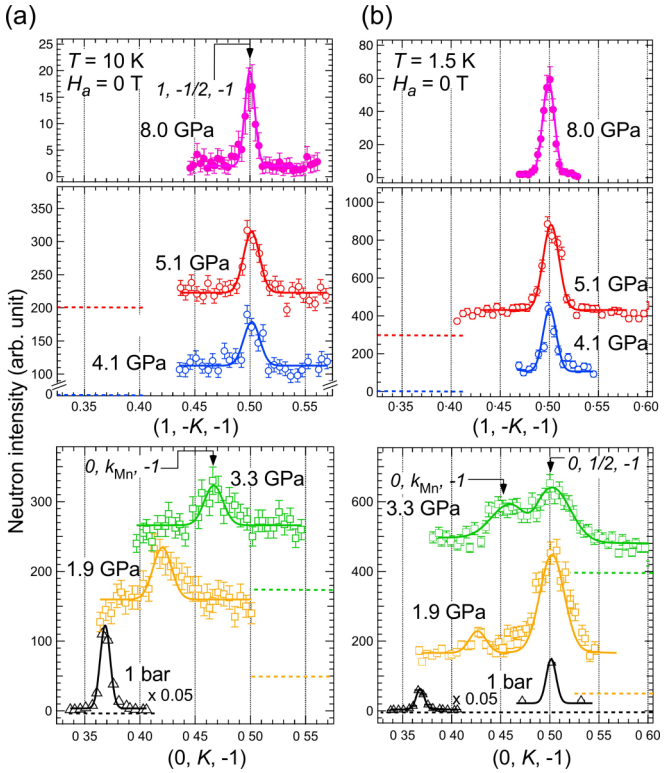

FIG. 3. Typical magnetic neutron diffraction profiles in the *x-x* channel for a polarized neutron experiment below 5.1 GPa, and for an unpolarized neutron experiment at 8.0 GPa, along the reciprocal lattice lines $[0, K, -1]$ and $[1, -K, -1]$ obtained at several pressures at (a) 10 K and (b) 1.5 K. The data denoted by triangle, square, and circle symbols were measured with sample 2 without the pressure cell and sample 1 inside the cell. The dotted horizontal lines in (a) and (b) denote zero lines for each profile. The data for 8.0 GPa were subtracted by those measured in the paramagnetic phase at 50 K.

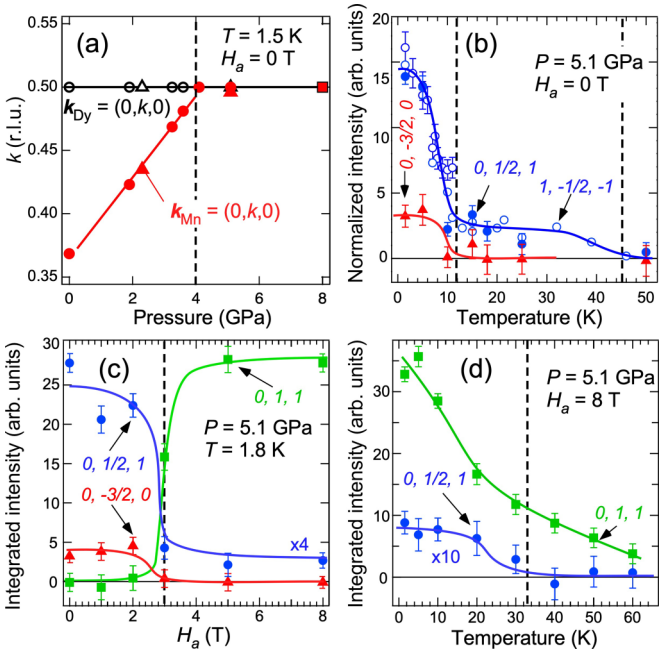

FIG. 4. (a) Pressure dependence of the propagation wave number k in the $\boldsymbol{k}$ vector for Mn (solid) and Dy (open) orderings. Here, "r.l.u" is an abbreviation for "reciprocal lattice unit." Circles, triangles, and squares denote the data measured on IN20, WISH, and Cyclops, respectively. (b) Temperature dependence of the magnetic neutron intensities for typical reflections at 5.1 GPa. The data measured on WISH (solid) and IN20 (open) instruments are normalized to each other by data collected at $T = 5$ K. (c) Magnetic field dependence of the integrated intensity of $0-\frac{3}{2}0$, $0\frac{1}{2}1$, and 011 magnetic reflections, at $T = 1.8$ K and $P = 5.1$ GPa. (d) Temperature dependence of $0\frac{1}{2}1$, and 011 magnetic reflections at $H_a = 8$ T and $P = 5.1$ GPa. The data in (c) and (d) were measured on WISH.

observed at $T = 10$ K at ambient pressure, and gradually shifted below $P = 4.0$ GPa. The k value is locked into commensurate $\frac{1}{2}$ above $P = 4.0$ GPa up to $P = 8.0$ GPa, as shown in Figs. 3(a) and 4(a). We thus find that the incommensurate to commensurate phase transition for Mn spins is consistent with the macroscopic measurement [4]. At $T = 1.5$ K, in addition to the reflection seen at $T = 10$ K, the reflections at $\boldsymbol{Q} = (0, \frac{1}{2}, -1)$ and $\boldsymbol{Q} = (1, \frac{1}{2}, -1)$, assigned by the commensurate $\boldsymbol{k}_{\mathrm{Dy}} = (0, \frac{1}{2}, 0)$, are observed for all pressures measured, as shown in Figs. 3(b) and 4(a). The onset of commensurate reflections below $T \sim 50$ K at $P = 5.1$ GPa and significantly enhanced below $T \sim 12$ K is due to the additional Dy order [Fig. 4(b)].

When the magnetic field is applied along the a axis (H_a) at $P = 5.1$ GPa, the magnetic reflection at $(0, \frac{3}{2}, 0)$ associated with the Dy order disappears at $H_a = 3$ T, as shown in Figs. 4(c) and 5(a). The $0\frac{1}{2}1$ reflection contributed by the Mn order has nonzero intensity even above $H_a = 3$ T [Fig. 5(b)]. In addition, the 011 reflection (forbidden in $Pbnm$) is induced. The critical H_a at $P = 5.1$ GPa is consistent with the field at which the ferroelectric polarization is largely enhanced [4]. At $H_a = 8$ T and $P = 5.1$ GPa, the $0\frac{1}{2}1$ reflection disappears above $T \sim 30$ K, while the intensity of the 011 reflection is significantly reduced but does not disappear even above $T = 50$ K due to the induced uniform magnetization in the paramagnetic (PM) phase [Fig. 4(d)]. These experimental facts infer that the Dy order with $\boldsymbol{k}_{\mathrm{Dy}} = (0, \frac{1}{2}, 0)$ changes to the $\boldsymbol{k}_{\mathrm{Dy}} = (0, 0, 0)$ structure above $H_a = 3$ T, and the Mn order with $\boldsymbol{k}_{\mathrm{Mn}} = (0, \frac{1}{2}, 0)$ remains unchanged.

The H_a dependence of magnetic ordering for Dy spins is similarly seen in the low-pressure phase at $P = 2.3$ GPa. As shown in Figs. 5(c) and 5(d), the $0\frac{1}{2}1$ reflection disappears, while a crystallographically forbidden reflection at $\boldsymbol{Q} = (0, -1, 2)$ is induced above $H_a = 3$ T at $P = 2.3$ GPa. The incommensurate reflection at $\boldsymbol{Q} = (0, 0.44, 1)$, which is associated with Mn spin ordering, remains unchanged for $H_a \geqslant 3$ T. Considering the similar H_a effect on Dy ordering seen in the low- and high-pressure phase, we can infer that the Dy ordering at ambient pressure does not drastically change by application of pressure.

B. Magnetic structure analysis

The magnetic structure determinations were performed by the SNP analysis measurements and symmetry considerations. We first introduce the results for measurements at ambient pressure for the comparison. At ambient pressure, for the reflections assigned by $\boldsymbol{k}_{\mathrm{Mn}} = \boldsymbol{k}_{\mathrm{Dy}} = (0, 0.37, 0)$ at $T = 10$ K, the measured polarization matrix elements are

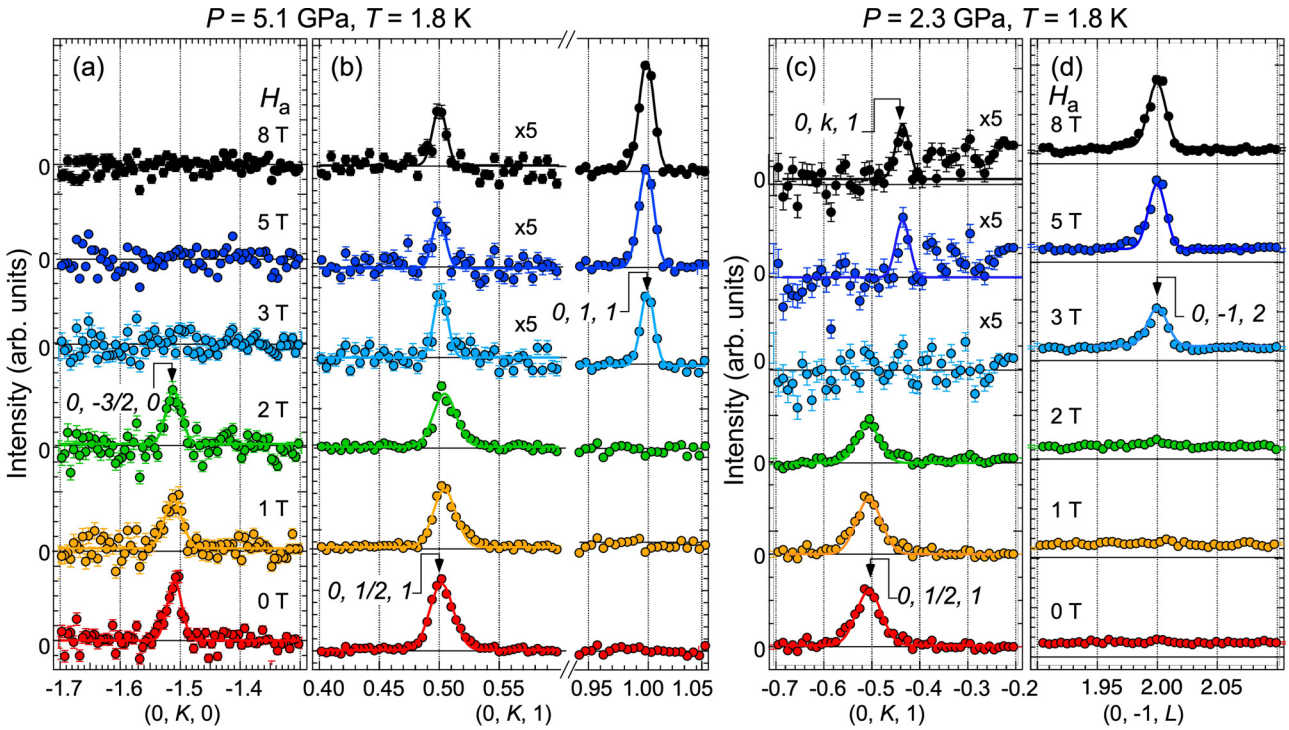

FIG. 5. Magnetic field dependence of the magnetic neutron diffraction pattern for $P = 5.1$ GPa for (a) and (b), and $P = 2.3$ for (c) and (d), at 1.8 K. The data in (a), (b), and (c) were subtracted by the data taken at the paramagnetic phase. The data were measured on WISH.

in good agreement with the reported magnetic structure [Fig. 6(a)]: a *bc*-cycloid structure with an ellipsoidal ratio $m_b/m_c = 2.5$ for the Mn spins [14] and collinear sinusoidal structure with spins along the *b* axis for Dy order [7]. For the Dy order with $\boldsymbol{k}_{\mathrm{Dy}} = (0, \frac{1}{2}, 0)$ below $T_{\mathrm{N}}^{\mathrm{Dy}}$, the noncollinear spin arrangement with *a* and *b* components with the ratio $m_a/m_b = 0.54 \pm 0.01$ explains the observed matrix elements at $T = 1.5$ K and ambient pressure [Fig. 6(b)]. The magnetic structure of Dy ordering is consistent with that reported in previous powder neutron diffraction measurements [7].

The symmetry analysis for the high-pressure phases with $\boldsymbol{k} = (0, \frac{1}{2}, 0)$ identified two two-dimensional irreducible representations (IRs), mX_1 and mX_2, at the Mn(4*a*) and Dy(4*c*) sites [23,24]. For this analysis, we selected IRs that restrict the electric polarization such that it is only along the *a* axis. For Mn ordering at $T = 15$ K at $P = 5.1$ GPa, the magnetic reflections are observed for $\boldsymbol{Q} = (m, n, l) \pm \boldsymbol{k}_{\mathrm{Mn}}$ with $l =$ odd, while it is not observed for $l =$ even [Fig. 4(b)], corresponding to an antiferromagnetic arrangement along the *c* axis. These conditions restrict the magnetic structure for Mn order into either $(m_a, m_b, 0)$ for the mX_1 or $(0, 0, m_c)$ for the mX_2. In the SNP measurement at $T = 15$ K and $P = 5.1$ GPa, we observed $P_{yz} = -0.03 \pm 0.05$ and $P_{zz} = -1.02 \pm 0.07$ for $\boldsymbol{Q} = (-1, -\frac{1}{2}, 1)$. As shown in Fig. 6(c), the possibility for a $(0, 0, m_c)$ model for mX_2 can be excluded. The experimental data are in good agreement with one of the modes for an order parameter direction (OPD), (a, a) in mX_1 [23,24], which corresponds to the *E*-type ordering with Mn spins parallel to the *b* axis. This model gives the calculated values of $P_{yz} = 0$ and $P_{zz} = -1.00$. The accuracy of the spin canting from the *b* axis toward the $\pm a$ axis was estimated to be $\pm 15^\circ$. The magnetic space group for the *E*-type ordering was polar $P_b mn2_1$ [with a basis (0, 0, 1), (0, 2, 0), (−1, 0, 0)], allowing a spontaneous polarization along the *a* axis in the *Pbnm* setting.

For $T = 1.5$ K and $P = 5.1$ GPa, the additional reflections on $\boldsymbol{Q} = (m, n, l) \pm \boldsymbol{k}_{\mathrm{Dy}}$ with $l =$ even due to Dy order [shown in Fig. 4(b)] appears below $T_{\mathrm{N}}^{\mathrm{Dy}}$. Assuming that the *E*-type magnetic ordering for Mn spins [Fig. 6(c)] with $\boldsymbol{M}_{\mathrm{Mn}} = (0, 4.0, 0)\mu_B$ is stable even below $T_{\mathrm{N}}^{\mathrm{Dy}}$, we found the noncollinear magnetic structure model for Dy spins with components $\boldsymbol{M}_{\mathrm{Dy}} = [3.6(6), 4.6(5), 0]\mu_B$ in the *ab* plane fits the experimentally observed matrix elements at $T = 1.5$ K and $P = 5.1$ GPa [Fig. 6(d)]. The spin direction of Dy spins at $P = 5.1$ GPa, $m_a/m_b = 0.78 \pm 0.13$, is slightly different from $m_a/m_b = 0.54 \pm 0.01$ at ambient pressure. The determined magnetic ordering for Dy spins (mX_2) with the *E*-type Mn ordering (mX_1) is expressed as a combination of two IRs $mX_1 \oplus mX_2$ with order parameter directions (a, a) and (b, b), respectively [23,24]. The resultant magnetic space group is $P_a 2_1$, which allows polarization only along the *a* axis in the *Pbnm* setting.

For the magnetic structure of Dy spins in $H_a \geqslant 3$ T, $T \leqslant 10$ K, and $P \geqslant 4$ GPa, there is only one IR, allowing a ferromagnetic component along the *a* axis, for $\boldsymbol{k}_{\mathrm{Dy}} = (0, 0, 0)$ associated with the little group of *Pbnm*, which is $m\Gamma_2^+$ ($F_x C_y$ in Bertaut's notation [25]). Combining the Dy ordering with the *E*-type Mn ordering, $m\Gamma_2^+ \oplus mX_1$, we obtained the magnetic space group $Pn'a2_1$ [with a basis (0,2,0), (0,0,1), (1,0,0) in the *Pbnm* setting], which allows ferroelectric polarization only along the *a* axis.

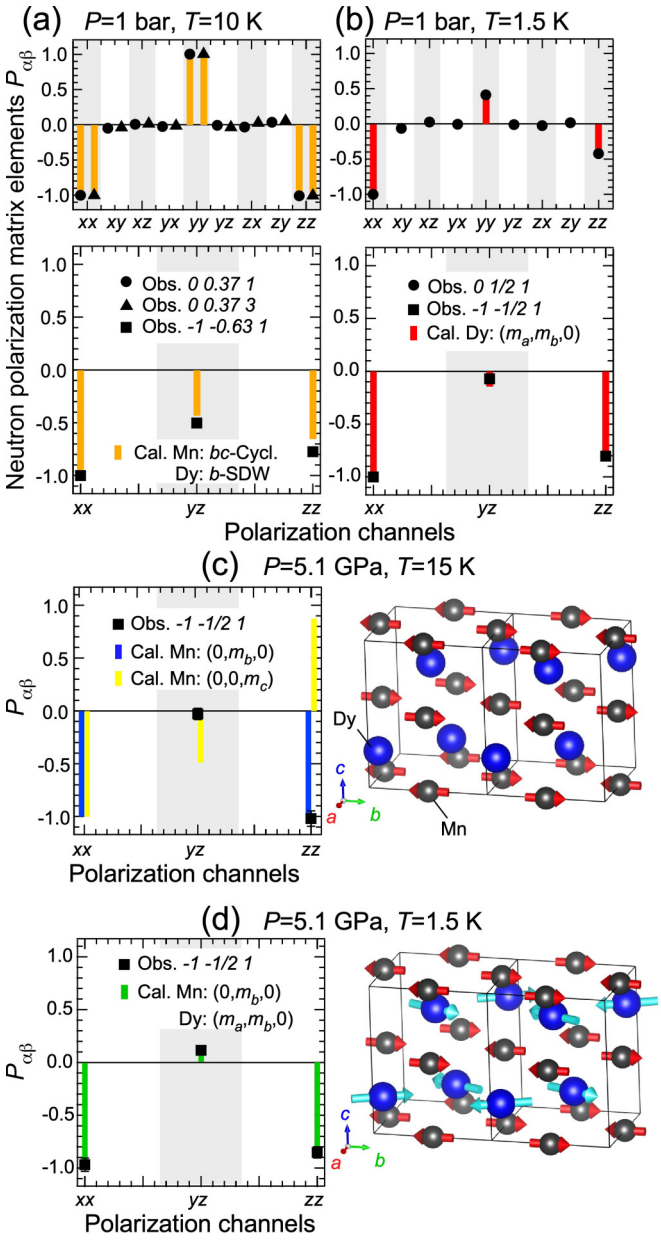

FIG. 6. Comparisons between observed and calculated polarization matrix elements $P_{\alpha\beta}$ for (a) the 0 0.37 1, 0 0.37 3, and -1 $-$ 0.63 1 reflections at $T = 10$ K, (b) the $0\frac{1}{2}1$ and $-1\frac{1}{2}1$ reflections at $T = 1.5$ K at ambient pressure, and the $-1\frac{1}{2}1$ reflection at (c) $T =$ 15 K and (d) $T = 1.5$ K for $P = 5.1$ GPa. The magnetic structures determined at (c) $T = 15$ K and (d) $T = 1.5$ K in $P = 5.1$ GPa are illustrated.

IV. DISCUSSION

Let us discuss the relationship between magnetic orderings and ferroelectric polarization in the high-pressure phases of $DyMnO_3$. It should be noted that there is no purely structural distortion induced by pressure up to 8 GPa, reported in previous high-pressure x-ray experiments at room temperature in $RMnO_3$ (R = Gd, Dy, Tb) [26–28]. The gigantic ferroelectric polarization along the a axis in $DyMnO_3$, $\sim$1.0 μC/cm^2, which appears below $T \sim 30$ K for the pressure region above 4.0 GPa, can be explained by the exchange striction mechanism for the E-type magnetic ordering for Mn spins [4,29,30]. However, the large polarization is significantly reduced below T_N^{Dy} to $\sim$0.3 μC/cm^2 in zero magnetic field [4]. The polarization is recovered to the maximum value $\sim$1.0 μC/cm^2 by application of a magnetic field for $H_a \geqslant$ 3 T [4]. The present neutron diffraction experiment proved that the large polarization changes in H_a and temperature are associated with the Dy spin ordering. The total polarization P_a can be expressed by the three terms for the exchange striction mechanism, $P_a = \sum_{ij} \alpha_{ij}(\boldsymbol{S}_i^{Mn} \cdot \boldsymbol{S}_j^{Mn}) + \sum_{ij} \beta_{ij}(\boldsymbol{S}_i^{Dy} \cdot \boldsymbol{S}_j^{Dy}) + \sum_{ij} \gamma_{ij}(\boldsymbol{S}_i^{Dy} \cdot \boldsymbol{S}_j^{Mn})$. The first term corresponds to the polar lattice distortion with $\boldsymbol{k}_{lattice} = 2\boldsymbol{k}_{Mn} = (0, 0, 0)$ induced by the E-type Mn ordering, which corresponds to a polar mode in Γ_2^- in $Pbnm$. The second term for Dy-Dy exchange bonds also generates the same polar mode, but can be ignored. Because the Dy ordering below T_N^{Dy} in the high-pressure phase at $H_a =$ 0 is similar and the same symmetry to the ambient pressure, which does not affect polarization along the a axis [9]. The Dy ordering for $H_a \geqslant 3$ T and $P \geqslant 4$ GPa (F_xC_y) becomes nonpolar $Pbn'm'$, which does not affect the polarization.

The incommensurate lattice distortion with the $\boldsymbol{k}$ vector $=$ $(0, 0.905, 0)$ has been reported in previous resonant x-ray diffraction experiments at ambient pressure [7,11]. It can be explained as the exchange striction for Dy-Mn bonds, corresponding to the third term, assigned by the combination of the incommensurate $\boldsymbol{k}$ vectors, $\boldsymbol{k}_{lattice} = \boldsymbol{k}_{Mn} + \boldsymbol{k}_{Dy} \simeq (0, 0.9, 0)$ [31]. This distortion does not cause uniform electric polarization due to the incommensurately oscillating distortion at ambient pressure. On the other hand, the lattice distortion modulation becomes $\boldsymbol{k}_{lattice} = \boldsymbol{k}_{Mn} + \boldsymbol{k}_{Dy} = (0, 0, 0)$ in the high-pressure phase. If the $\boldsymbol{k}_{lattice} = (0, 0, 0)$ distortion is polar, it can cause a significant change in the polarization below T_N^{Dy}. Moreover, the magnetic field changes the Dy ordering from $\boldsymbol{k}_{Dy} = (0, \frac{1}{2}, 0)$ to (0,0,0) above $H_a = 3$ T, leading to the other distortion mode, $\boldsymbol{k}_{Mn} + \boldsymbol{k}_{Dy} = (0, \frac{1}{2}, 0)$, without a contribution of polarization. Therefore, the polarization value $P_a \sim 1.0$ μC/cm^2 of the first term can be retrieved above $H_a \geqslant 3$ T due to the absence of the negative contribution originating from the third term.

For a comparison with $TbMnO_3$, Tb ordering in the high-pressure phase was reported to be $\boldsymbol{M}_{Tb} =$ $[5.9(3), 1.8(8), 0]\mu_B$ in the same structure as the Dy one [6]. The magnetic field enhancement of polarization for $DyMnO_3$, $\Delta P_a^{Dy} = |P_a^{Dy}(8\text{ T}) - P_a^{Dy}(0\text{ T})|/P_a^{Dy}(8\text{ T}) \sim 0.70$, is larger than that for $TbMnO_3$, $\Delta P_a^{Tb} \sim 0.36$ [3,4]. The smaller spin b component of Tb spins can give less of an exchange striction effect between the rare earth and Mn spins in $TbMnO_3$ than $DyMnO_3$, which can be estimated to be $|\boldsymbol{S}_i^{Tb} \cdot \boldsymbol{S}_j^{Mn}|/|\boldsymbol{S}_i^{Dy} \cdot \boldsymbol{S}_j^{Mn}| = 0.39 \pm 0.16$. This value is approximately consistent with $\Delta P_a^{Tb}/\Delta P_a^{Dy} \sim 0.51$. We thus conclude that the exchange striction for rare earth and Mn bonds in the high-pressure phase of $RMnO_3$ is strongly related to the electric polarization enhancement by application of H_a.

However, it should be noted that the situation for the exchange striction for Dy(Tb)-Mn bonds is more complicated, because the exchange striction for the combination of the different magnetic IRs, mX_1 for Mn and mX_2 for Dy(Tb), in the high-pressure phase generates only two nonpolar distortion

modes in Γ_1^- and Γ_2^+ in *Pbnm* [23,24]. The Γ_1^- distortion individually breaks some of the symmetry elements in *Pbnm* and causes the crystal to be piezoelectric $P2_12_12_1$. The Γ_2^+ alone breaks the symmetry down to $P2_1/c$ as a monoclinic strain. Therefore, those distortions separately do not generate uniform polarization. Although a combination of the piezoelectric distortion of Γ_1^- and the Γ_2^+ strain can generate the polarization, it is expected to be much smaller than that induced by the exchange striction for Mn-Mn bonds, because the polarization of the Γ_1^- and Γ_2^+ combination is proportional to the product of the small magnetoelastic distortions. If one of the distortions, Γ_1^- and Γ_2^+, preexists independently of the magnetic order in the crystal lattice, the exchange striction for rare earth and Mn bonds could induce the large polarization changes. High-resolution x-ray diffraction under high pressure is needed to make this point clear.

V. CONCLUSION

In conclusion, we have determined the magnetic structures in the high-pressure phase with giant ferroelectric polarization in $DyMnO_3$. For Mn spins, the E-type magnetic ordering with $\boldsymbol{k}_{\mathrm{Mn}} = (0, \frac{1}{2}, 0)$ is stabilized above 4.0 GPa, which induces the giant ferroelectric polarization through the exchange striction effect. The magnetic ordering for the Dy spins below $T_{\mathrm{N}}^{\mathrm{Dy}}$, which was determined to be the noncollinear spin arrangement with $\boldsymbol{k}_{\mathrm{Dy}} = (0, \frac{1}{2}, 0)$, almost remains unchanged even above 4.0 GPa. The magnetic field along the a axis changes the magnetic structure of Dy spins into the $\boldsymbol{k} = (0, 0, 0)$ structure above $H_a = 3$ T, which is concomitant with the large magnetic field enhancement of the ferroelectric polarization [4]. Considering the exchange striction for the three types of exchange bonds in $DyMnO_3$, we conclude that the lattice distortion associated with the exchange striction for the rare earth and Mn bonds is strongly related to the significant magnetic field enhancement of ferroelectric polarization in the rare earth manganites. Finally, it is our hope that the feasibility of the present SNP experiment under high pressure will encourage researchers to investigate pressure-induced physical phenomena associated with complex magnetic ordering.

ACKNOWLEDGMENTS

We would like to thank Jérôme Debray in Institut Néel/CNRS for technical support by cutting and polishing the crystals. The images in Fig. 6 were depicted by the VESTA [32] program. We acknowledge the STFC and ILL for access to neutron beamtime. This work was supported by JSPS KAKENHI Grants No. 15H05433 and No. 17KK0099, JST-Mirai Program Grant No. JPMJMI18A3, Japan, and the TUMOCS project, which has received funding from the European Union Horizon 2020 Research and Innovation Program under the Marie Sklodowska-Curie Grant Agreement No. 645660.

[1] T. Kimura, T. Goto, H. Shintani, K. Ishizaka, T. Arima, and Y. Tokura, Nature (London) **426**, 55 (2003).
[2] S.-W Cheong and M. Mostovoy, Nat. Mater. **6**, 13 (2007).
[3] T. Aoyama, K. Yamauchi, A. Iyama, S. Picozzi, K. Shimizu, and T. Kimura, Nat. Commun. **5**, 4927 (2014).
[4] T. Aoyama, A. Iyama, K. Shimizu, and T. Kimura, Phys. Rev. B **91**, 081107(R) (2015).
[5] O. L. Makarova, I. Mirebeau, S. E. Kichanov, J. Rodriguez-Carvajal, and A. Forget, Phys. Rev. B **84**, 020408(R) (2011).
[6] N. Terada, D. D. Khalyavin, P. Manuel, T. Osakabe, A. Kikkawa, and H. Kitazawa, Phys. Rev. B **93**, 081104(R) (2016).
[7] O. Prokhnenko, R. Feyerherm, E. Dudzik, S. Landsgesell, N. Aliouane, L. C. Chapon, and D. N. Argyriou, Phys. Rev. Lett. **98**, 057206 (2007).
[8] R. Feyerherm, E. Dudzik, A. U. B. Wolter, S. Valencia, O. Prokhnenko, A. Maljuk, S. Landsgesell, N. Aliouane, L. Bouchenoire, S. Brown, and D. N. Argyriou, Phys. Rev. B **79**, 134426 (2009).
[9] T. Kimura, S. Ishihara, H. Shintani, T. Arima, K. T. Takahashi, K. Ishizaka, and Y. Tokura, Phys. Rev. B **68**, 060403(R) (2003).
[10] T. Kimura, G. Lawes, T. Goto, Y. Tokura, and A. P. Ramirez, Phys. Rev. B **71**, 224425 (2005).
[11] R. Feyerherm, E. Dudzik, N. Aliouane, and D. N. Argyriou, Phys. Rev. B **73**, 180401(R) (2006).
[12] R. Kajimoto, H. Yoshizawa, H. Shintani, T. Kimura, and Y. Tokura, Phys. Rev. B **70**, 012401 (2004).
[13] M. Kenzelmann, A. B. Harris, S. Jonas, C. Broholm, J. Schefer, S. B. Kim, C. L. Zhang, S-W. Cheong, O. P. Vajk, and J. W. Lynn, Phys. Rev. Lett. **95**, 087206 (2005).
[14] T. Arima, A. Tokunaga, T. Goto, H. Kimura, Y. Noda, and Y. Tokura, Phys. Rev. Lett. **96**, 097202 (2006).
[15] F. Tasset, Physica B **156-57**, 627 (1989).
[16] F. Tasset, P. J. Brown, E. Lelièvre-Berna, T. Roberts, S. Pujol, J. Allibon, and E. Bourgeat-Lami, Physica B **267-268**, 69 (1999).
[17] J. A. Blanco, P. J. Brown and A. Stunault, K. Katsumata, F. Iga, and S. Michimura, Phys. Rev. B **73**, 212411 (2006).
[18] N. Terada, N. Qureshi, L. C. Chapon, and T. Osakabe, Nat. Commun. **9**, 4368 (2018).
[19] N. Terada, Trans. Mater. Res. Soc. Jpn. **44**, 1 (2019).
[20] N. Qureshi, J. Appl. Crystallogr. **52**, 175 (2019).
[21] L. C. Chapon, P. Manuel, P. G. Radaelli, C. Benson, L. Perrott, S. Ansell, N. J. Rhodes, D. Raspino, D. Duxbury, E. Spill, and J. Norris, Neutron News **22**, 22 (2011).
[22] R. L. Cook, H. E. King, Jr., C. A. Herbst, and D. R. Herschbach, J. Chem. Phys. **100**, 5178 (1994).
[23] B. J. Campbell, H. T. Stokes, D. E. Tanner, and D. M. Hatch, J. Appl. Crystallogr. **39**, 607 (2006).
[24] J. M. Perez-Mato, J. L. Ribeiro, V. Petricek, and M. I. Aroyo, J. Phys.: Condens. Matter **24**, 163201 (2012).
[25] E. F. Bertaut, in *Magnetism*, edited by G. T. Rado and H. Suhl (Academic, New York, 1963), p. 149.
[26] J. M. Chen, T. L. Chou, J. M. Lee, S. A. Chen, T. S. Chan, T. H. Chen, K. T. Lu, W. T. Chuang, H.-S. Sheu, S. W. Chen, C. M. Lin, N. Hiraoka, H. Ishii, K. D. Tsuei, and T. J. Yang, Phys. Rev. B **79**, 165110 (2009).
[27] J. M. Chen, J. M. Lee, T. L. Chou, S. A. Chen, S. W. Huang, H. T. Jeng, K. T. Lu, T. H. Chen, Y. C. Liang, S. W. Chen, W. T. Chuang, H.-S. Sheu, N. Hiraoka, H. Ishii, K. D. Tsuei,

E. Huang, C. M. Lin, and T. J. Yang, J. Chem. Phys. **133**, 154510 (2010).

[28] C. Lin, Y. Zhang, J. Liu, X. Li, Y. Li, L. Tang, and L. Xiong, J. Phys.: Condens. Matter **24**, 115402 (2012).

[29] I. A. Sergienko, C. Sen, and E. Dagotto, Phys. Rev. Lett. **97**, 227204 (2006).

[30] S. Picozzi, K. Yamauchi, B. Sanyal, I. A. Sergienko, and E. Dagotto, Phys. Rev. Lett. **99**, 227201 (2007).

[31] R. Feyerherm, E. Dudzik, O. Prokhnenko, and D. N. Argyriou, J. Phys.: Conf. Ser. **200**, 012032 (2010).

[32] K. Momma and F. Izumi, J. Appl. Crystallogr. **41**, 653 (2008).